NASA/TM—2019-219731

IEPC–2017–207

Wear Trends of the HERMeS Thruster as a Function of Throttle Point

George J. Williams, Jr., Hani Kamhawi, Maria Choi, Thomas W. Haag, Wensheng Huang, and Daniel A. Herman
Glenn Research Center, Cleveland, Ohio

James H. Gilland
Ohio Aerospace Institute, Brook Park, Ohio

Peter Y. Peterson
Vantage Partners, LLC, Brook Park, Ohio

April 2019

NASA STI Program . . . in Profile

Since its founding, NASA has been dedicated to the advancement of aeronautics and space science. The NASA Scientific and Technical Information (STI) Program plays a key part in helping NASA maintain this important role.

The NASA STI Program operates under the auspices of the Agency Chief Information Officer. It collects, organizes, provides for archiving, and disseminates NASA's STI. The NASA STI Program provides access to the NASA Technical Report Server—Registered (NTRS Reg) and NASA Technical Report Server—Public (NTRS) thus providing one of the largest collections of aeronautical and space science STI in the world. Results are published in both non-NASA channels and by NASA in the NASA STI Report Series, which includes the following report types:

- TECHNICAL PUBLICATION. Reports of completed research or a major significant phase of research that present the results of NASA programs and include extensive data or theoretical analysis. Includes compilations of significant scientific and technical data and information deemed to be of continuing reference value. NASA counter-part of peer-reviewed formal professional papers, but has less stringent limitations on manuscript length and extent of graphic presentations.

- TECHNICAL MEMORANDUM. Scientific and technical findings that are preliminary or of specialized interest, e.g., "quick-release" reports, working papers, and bibliographies that contain minimal annotation. Does not contain extensive analysis.

- CONTRACTOR REPORT. Scientific and technical findings by NASA-sponsored contractors and grantees.

- CONFERENCE PUBLICATION. Collected papers from scientific and technical conferences, symposia, seminars, or other meetings sponsored or co-sponsored by NASA.

- SPECIAL PUBLICATION. Scientific, technical, or historical information from NASA programs, projects, and missions, often concerned with subjects having substantial public interest.

- TECHNICAL TRANSLATION. English-language translations of foreign scientific and technical material pertinent to NASA's mission.

For more information about the NASA STI program, see the following:

- Access the NASA STI program home page at http://www.sti.nasa.gov

- E-mail your question to help@sti.nasa.gov

- Fax your question to the NASA STI Information Desk at 757-864-6500

- Telephone the NASA STI Information Desk at 757-864-9658

- Write to:
  NASA STI Program
  Mail Stop 148
  NASA Langley Research Center
  Hampton, VA 23681-2199

NASA/TM—2019-219731 IEPC–2017–207

Wear Trends of the HERMeS Thruster as a Function of Throttle Point

George J. Williams, Jr., Hani Kamhawi, Maria Choi, Thomas W. Haag, Wensheng Huang, and Daniel A. Herman
Glenn Research Center, Cleveland, Ohio

James H. Gilland
Ohio Aerospace Institute, Brook Park, Ohio

Peter Y. Peterson
Vantage Partners, LLC, Brook Park, Ohio

Prepared for the
35th International Electric Propulsion Conference
sponsored by the Electric Rocket Propulsion Society
Atlanta, Georgia, October 8–12, 2017

National Aeronautics and
Space Administration

Glenn Research Center
Cleveland, Ohio 44135

April 2019

Acknowledgments

The authors thank the Space Technology Mission Directorate through the Solar Electric Propulsion (SEP) Technology Demonstration Mission Project for funding the joint NASA Glenn Research Center (GRC) and Jet Propulsion Laboratory development of the Advanced Electric Propulsion System (AEPS). The authors thank Todd Tofil for managing the electric propulsion work within the SEP Project and Richard Hofer for leading the AEPS thruster development effort. The authors also thank the many NASA/Aerojet review board members and subject matter experts for providing their expertise and technical guidance to the development of AEPS and its broader Ion Propulsion Subsystem mission application. The authors also thank the engineers and technicians of the Space Facilities Branch at GRC who enabled all of the test results presented herein.

Level of Review: This material has been technically reviewed by technical management.

Available from

NASA STI Program
Mail Stop 148
NASA Langley Research Center
Hampton, VA 23681-2199

National Technical Information Service
5285 Port Royal Road
Springfield, VA 22161
703-605-6000

This report is available in electronic form at http://www.sti.nasa.gov/ and http://ntrs.nasa.gov/

Wear Trends of the HERMeS Thruster as a Function of Throttle Point

George J. Williams, Jr., Hani Kamhawi, Maria Choi,
Thomas W. Haag, Wensheng Huang, and Daniel A. Herman
National Aeronautics and Space Administration
Glenn Research Center
Cleveland, Ohio 44135

James H. Gilland
Ohio Aerospace Institute
Brook Park, Ohio 44142

Peter Y. Peterson
Vantage Partners, LLC
Brook Park, Ohio 44142

Abstract

A series of short-duration (200 h) wear tests were conducted with two HERMeS technology demonstration units. Front pole covers, cathode keeper, and discharge channel wear were characterized as a function of discharge voltage, magnetic field strength, and chamber pressure. No discharge channel erosion was observed. Inner pole cover erosion was shown to be a weak function of discharge voltage with most erosion occurring at the lowest value, 300 V. The TDU-3 keeper electrode eroded with each operating condition, with high magnetic field yielding the greatest erosion rate. The TDU-1 keeper electrode exhibited net deposition suggesting its configuration is more consistent with meeting overall HERMeS service life requirements. Ratios of molybdenum to graphite erosion rates suggests, with high uncertainty, that the sputtering ions are originating downstream of the thruster exit plane, striking the surface with small angles of incidence.

Nomenclature

AEPS	Advanced Electric Propulsion System
HERMeS	Hall Effect Rocket with Magnetic Shielding
IFPC	Inner Front Pole Cover
J_b	body current, A
J_d	discharge current, A
OFPC	Outer Front Pole Cover
TC	Test Condition
TDU	Technology Demonstration Unit
p-p	peak-to-peak
QCM	Quartz Crystal Microbalance
V_{cg}	cathode to ground voltage, V
V_d	discharge voltage, V
VF	Vacuum Facility
V_k	keeper voltage, V

1.0 Introduction

For missions beyond low Earth orbit, spacecraft size and mass can be dominated by onboard chemical propulsion systems and propellants that may constitute more than 50 percent of spacecraft mass. This impact can be substantially reduced through the utilization of Solar Electric Propulsion (SEP) due to its substantially higher specific impulse. Studies performed for NASA's Human Exploration and Operations Mission Directorate and Science Mission Directorate have demonstrated that a 40 kW-class SEP capability can be enabling for both near term and future architectures and science missions (Ref. 1). Since 2012 NASA has been developing a 14 kW Hall thruster electric propulsion string that can serve as the building block for realizing a 40 kW-class SEP capability. NASA continues to evolve a human exploration approach to expand human presence beyond low-Earth orbit and to do so, where practical, in a manner involving international, academic, and industry partners (Ref. 1). NASA publicly presented a phased exploration concept at the Human Exploration and Operations (HEO) Committee of the NASA Advisory Council meeting on March 28, 2017 (Ref. 2). NASA presented an evolutionary human exploration architecture, depicted in Figure 1, to expand human presence deeper into the solar system through a phased approach including cis-lunar flight testing and validation of exploration capability before crewed missions beyond the earth-moon system and eventual crewed Mars missions. One of the key objectives is to achieve human exploration of Mars and beyond through the prioritization of those technologies and capabilities best suited for such a mission in accordance with the stepping stone approach to exploration (Ref. 3). High-power solar electric propulsion is one of those key technologies that has been prioritized because of its significant exploration benefits. A high-power, 40 kW-class Hall thruster propulsion system provides significant capability and represents, along with flexible blanket solar array technology, a readily scalable technology with a clear path to much higher power systems.

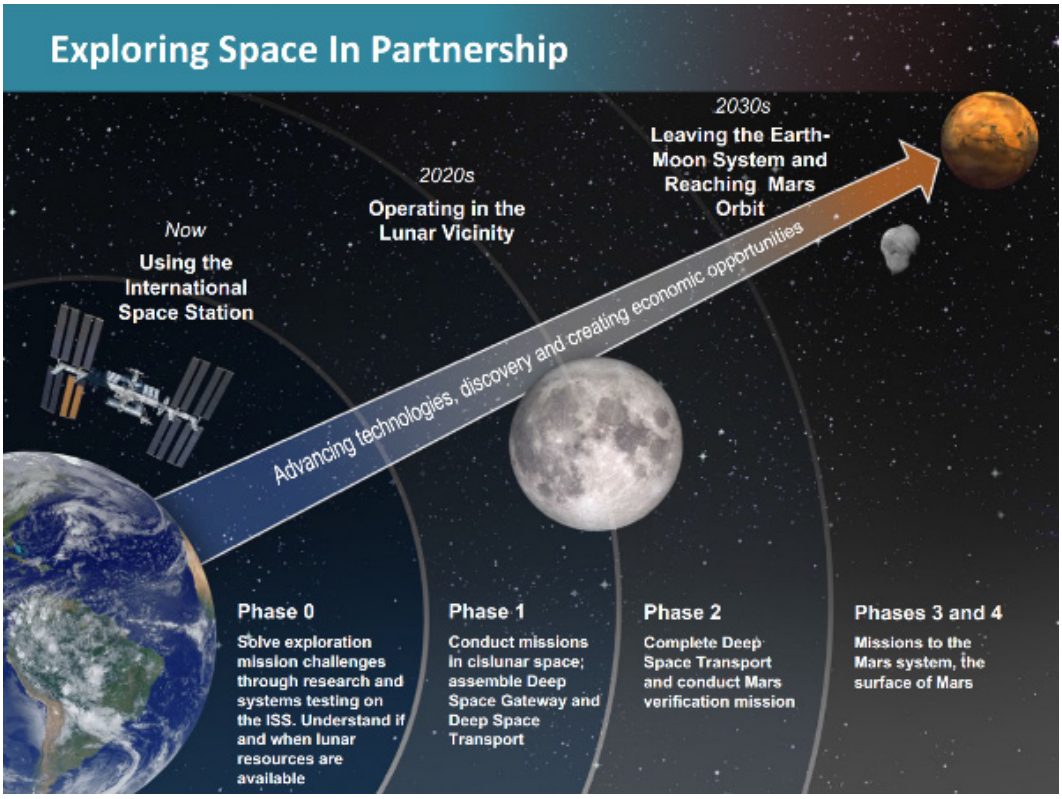

Figure 1.—Deep Space Gateway and Transport Plan depiction (Ref. 3).

The 14 kW Hall thruster system development, led by the NASA Glenn Research Center (GRC) and the Jet Propulsion Laboratory (JPL), began with maturation of the high-power Hall thruster and power processing unit. The technology development work has transitioned to Aerojet Rocketdyne via a competitive procurement selection for the Advanced Electric Propulsion System (AEPS). The AEPS contract includes the development, qualification, and multiple flight 14 kW electric propulsion string deliveries. The AEPS EP string consists of the Hall thruster, power processing unit (including digital control and interface functionality), xenon flow controller, and associated intra-string harnesses. NASA continues to support the AEPS development leveraging in-house expertise, plasma modeling capability, and world-class test facilities. NASA also executes AEPS and mission risk reduction activities to support the AEPS development and mission application. An overview of the NASA and Aerojet development activities and mission application of the AEPS Hall thruster system is provided by Herman (Ref. 4).

With the introduction of the Hall-Effect Thruster with Magnetic Shielding (HERMeS) (Refs. 5 and 6), service life-limiting erosion of the boron nitride channel appears to have been eliminated (Refs. 7, 8, 9, and 10). However, erosion of other surfaces was increased resulting in the incorporation of an engineering solution to mitigate the impact of the erosion which included incorporation of graphite front pole covers and thruster operation with the cathode electrically tied to the thruster body. Risk-reduction activities have continued to characterize the erosion of cathode-potential surfaces (including the cathode keeper). These include, surface layer activated wear testing (Ref. 11), extensive numerical modeling(Refs. 12 and 13), assessment of the impact of carbon deposition on service-life assessment(Ref. 14), laser-based characterization of near-field ions(Ref. 15), and a series of short duration wear tests which are discussed in this paper.

All of the risk-reduction activities to date have identified erosion of the inner front pole cover as the (new) erosion-based service life limit. Before developing the HERMeS into an engineering-level configuration and entering the long-duration and environmental testing, a test campaign at NASA JPL was undertaken to characterize the erosion of the inner front pole cover as a function of thruster throttle point and facility pressure. In order to conduct this campaign in a reasonable amount of time, surface activation of molybdenum pole covers was incorporated. Results showed the pole cover eroded more at lower discharge voltages, lower discharge currents, higher magnetic fields, and lower facility pressures (Ref. 11). Some of these trends were unexpected and numerical data suggested that some of the trends may not be observed in graphite pole covers because of graphite's much higher sputtering threshold (Ref. 13).

Because understanding how throttle level impacts service life is of great value to mission planners, long-duration testing of a high-fidelity laboratory model thruster was deferred so that a series of short duration wear tests could characterize the erosion of graphite inner pole covers as a function of operating condition. These tests would also be of sufficient length to characterize the impact of throttling on the erosion of other HERMeS surfaces such as the cathode keeper and the outer front pole cover. Sufficient performance characterization had already been conducted yielding no erosion of the boron nitride discharge channel. In addition to characterizing the thruster wear, the short-duration test campaign was intended to fully characterize the performance of the thruster which incorporated design changes since the previous wear test and to provide additional characterization of the test facility in support of very-long duration testing.

This paper presents the erosion trends of the HERMeS observed in seven short duration (~ 200 h) tests. As discussed below, two thruster configurations were tested in two different vacuum facilities at GRC. While performance trends associated with the erosion measurements are provided to facilitate discussion, detailed performance characterization is provided in a companion paper by Kamhawi (Ref. 16). A preliminary correlation of the graphite erosion with ambient plasma conditions (yielding the

erosion) is provided by comparing these erosion rates with those of molybdenum surfaces placed on the graphite. Comparisons to the SLA data and to prevailing plasma models are also made in the discussion of the data. However, consistent correlation of the various measurements with plasma properties remains a work in progress and will likely require leveraging additional risk-reduction testing planned in the near future.

2.0 Hardware and Technical Approach

2.1 Technology Demonstration Units

Two HERMeS technology demonstration units (TDU) were operated as part of this test campaign, TDU-1 and TDU-3. Kamhawi (Ref. 16) provides full discussion of the changes incorporated into TDU-3 based on lessons learned from both TDU-1 and TDU-2 testing and from collaboration with Aerojet Rocketdyne in the development of the engineering design units (EDU). Excepting, of course, the inner pole cover, TDU-1 was largely unchanged from its configuration as operated during the 2016 1700 h wear test. A different cathode assembly was incorporated, as the one from the TDU-1 wear test was incorporated into TDU-3 in preparation for its long duration testing. The electrical interfaces to both thrusters incorporated filtering which ensured that both thrusters operated at the same prescribed discharge voltage peak-to-peak values at 600 V, 12.5 kW operation.

Differences of note between the two TDU configurations included cathode axial location, discharge channel material, control of thermal interfaces, and magnetic coil configuration. Because the magnetic shielding configuration was predicted to result in higher erosion of the inner front pole cover than an unshielded configuration, thicker pole covers were incorporated on TDU-1 prior to its characterization and wear testing in 2016. This resulted in the downstream surface of the cathode's keeper electrode residing upstream of the downstream surface of the pole covers by roughly the thickness of the new pole covers. While the hollow cathode assembly (HCA) changed from 2016 to 2017 testing, its relative location in TDU-1 did not. The HCA incorporated into TDU-3 was modified to allow its keeper face to be in the plane of the downstream surfaces of the pole covers. The discharge channel in TDU-1 was unchanged from 2016, but that of TDU-3 was of a higher-fidelity grade of BN consistent with the EDU design. No performance difference was expected nor seen. Similarly, the magnetic coils of TDU-1 remained unchanged whereas TDU-3's were of a higher fidelity design consistent with the planned EDU. This resulted in different current settings to achieve the same magnetic field, but no change in the magnetic field shape for the same field strength. TDU-3's assembly reflected greater attention to minimizing surface contact thermal resistances which resulted in slightly lower steady-state temperatures.

Thermocouples were incorporated into both TDU-1 and TDU-3 to measure the temperatures of characteristic surfaces to validate and support thermal modeling of the thrusters. However, the HCA in TDU-3 incorporated two thermocouples providing temperatures of the cathode orifice plate and of the cathode tube at an upstream location. In addition to providing an indication of the HCA's insert life via numerical modeling17 the values also provide anchoring of the HCA wear testing ongoing in thruster simulators.

2.2 Space Simulation Facilities

TDU-3 was operated in Vacuum Facility 5 (VF-5) at GRC. A base pressure of $2 \cdot 10^{-7}$ Torr (air) was achieved throughout the campaign. Prior to the start of testing, the laboratory feed system passed a point of use purity check in accordance with the GRC's inspection and procedure document 305. This provided greater confidence that rate-of-rise tests ensured adequate purity of xenon delivered to the thruster. In all

respects not otherwise noted, the test configuration was identical to that used during the 1700 wear test (Ref. 9). Figure 2 shows TDU-3 mounted in VF-5 during the test campaign.

TDU-1 was operated in Vacuum Facility 6 (VF-6) at GRC. A base pressure of $9 \cdot 10^{-8}$ Torr (air) was achieved throughout the campaign. However, the pumping speed of VF-6 is roughly half that of VF-5 and TDU-1 operated at higher pressures than did TDU-3 in VF-5 for the same thruster operating condition. VF-6 was modified to accommodate AEPS testing as described in Peterson (Ref. 18). This included the fabrication of a thrust stand and assembly of a plasma probe rake identical to the one used in VF-5. An improved data acquisition and recording software suite was developed for VF-6 testing and then incorporated at VF-5. Figure 3 shows TDU-1 in VF-6 during the test campaign.

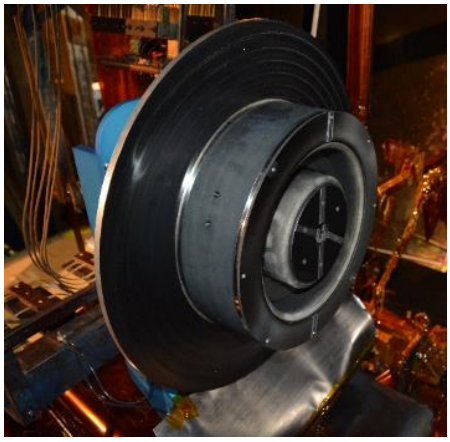

Figure 2.—TDU-3 in VF-5 configured for short-duration wear testing.

Electrical (plasma) paths to ground were eliminated within 1-m of the thruster in both facilities. The beam dump in VF-5 was floated. The equivalent surfaces in VF-6 were tied to ground. (TDU-1 wear testing in VF-5 in 2016 was conducted with the beam dump grounded.)

Graphite paneling or flexible sheets were incorporated on all surfaces exposed to the beam in both chambers to minimize the amount of back-sputtered material on the thruster. The internal surfaces of the stainless steel sleeves for the oil diffusion pumps were left exposed in VF-5 in anticipation of using the pumps during the course of the testing. The pumps were not used, but the exposed surfaces did result in slightly (10percent by mass) higher amounts of back-sputtered material during this test campaign compared to the previous 17000 h wear test.

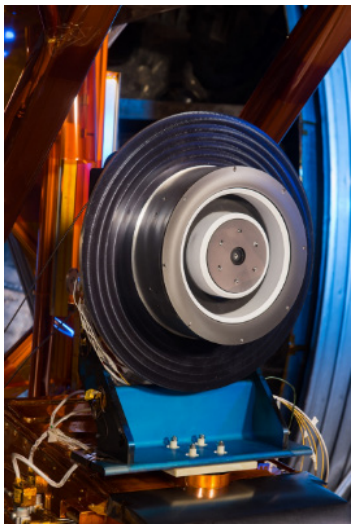

Figure 3.—TDU-1 in VF-6 configured for short-duration wear testing.

2.3 TDU Wear-Test Operating Conditions

The test campaign was constrained by test windows in both VF-5 and VF-6 and by the minimum time required to have reasonable signal to noise measurements of graphite erosion. From the inner pole cover erosion observed in the TDU-1 1700 h wear test segments, a nominal test duration of 175 to 200 h was established for the wear tests. A slightly shorter duration was accepted for the first 300 V 6.3 kW test based on SLA data that showed the erosion to be several times higher than that at other conditions (Ref. 11). A slightly longer duration was accepted for the 600 V, 12.5 kW test in VF-6 based on vacuum chamber availability and the expectation that the erosion at this condition would be the lowest of the series of tests.

Table I shows the seven tests that are included in this test campaign. Note that all tests were conducted at the nominal discharge current of 20.83 A. This corresponded to the nominal throttle curve developed for the now-cancelled Asteroid Redirect Robotic Mission (ARRM) (Ref. 4). The performance characterization test (TC-4) is included because a large fraction of the total thruster operation was at the 600 V, 12.5 kW nominal operation point. Also included in the table is the first segment of the TDU-1 wear test from 2016 (TC-0). It is included for reference as the erosion data for both Mo and graphite observed in the other tests are compared to the rates observed at this operating condition.

TABLE I.—THRUSTER OPERATING CONDITIONS (TC)

TC	TDU	VF	Vd, V	Magnetic field	V_{cg}, V	V_{cg}, p-p, V	V_k, V	V_k, p-p, V	J_d, p-p, A	V_d, p-p, V	J_b, A	p, μTorr	QCM, μm/kh	Time, h	Xe used, kg
0, 600 V	1	5	600	Nominal	–9.2	28	2.0	10	14	19	1.6	4.6	1.8	250	20.6
1, 300 V	3	5	300	Nominal	–9.2	14	2.3	7	7	12	0.92	5.0	2.2	165	12.3
2, 400 V	3	5	400	Nominal	–9.6	15	2.2	7	8	12	1.2	4.9	2.2	193	14.5
3, 500 V	3	5	500	Nominal	–9.3	27	1.8	12	15	24	1.5	4.9	2.2	196	15.6
4, 600 V	3	5	[a]600	Nominal	–8.8	28	2.1	10	15	29	1.7	4.9	2.2	182	15.2
5, 600 V	3	5	600	125% Nom.	–10	35	2.0	12	14	32	2.1	4.9	2.2	192	15.8
6, 300 V	1	6	300	Nominal	–9.5	14	1.2	7	7.2	13	0.94	11	0.45	191	14.2
7, 600 V	1	6	600	Nominal	–11	28	1.2	11	16	25	1.0	9.5	0.45	281	23.2

[a]TC-4, 600 V data were collected during the comprehensive performance characterization of TDU-3 during which time the thruster was operated over a range of discharge voltages, discharge currents, and magnetic field settings.

All wear testing and the vast majority of the performance characterization testing was conducted in the cathode-tied electrical configuration (Ref. 19). While it is a departure from previous flight Hall thrusters, this configuration is consistent with TDU-1 wear testing in 2016 and is the projected flight configuration.

2.4 Modification of Surfaces to Measure Erosion

In order to better characterize the erosion of the keeper downstream face, the inner front pole cover, and the outer front pole cover, masks were incorporated to provide unexposed (no erosion, no deposition) surfaces for post-test measurements. Molybdenum surfaces were also incorporated on each of these to provide accelerated erosion since the durations might not be sufficient to discern erosion on the keeper and outer front pole cover (based on TDU-1 2016 data) and to provide correlation with the SLA data collected at JPL since only a handful of the conditions tested in that campaign are repeated in this one. It was assumed that the masks would not impact the erosion rates of the masked surfaces.

2.4.1 Cathode Keeper Electrode

The keeper electrode in the TDU-1 1700 h wear test exhibited ambiguous erosion given there was no reference (unexposed) surface, but the erosion appeared to be small. The downstream surface of the keepers used in both TDU-1 and TDU-3 tests for this campaign were polished to provide a smooth surface to better capture the erosion over a short duration. Molybdenum masks were employed with each test to provide both masking and an accelerated erosion surface. The keeper was not removed after each test due to schedule constraints.

Figure 4 shows a Mo mask that was used to characterize the erosion of the keeper electrode. The mask incorporated a notch that exposed the underlying graphite surface and an orifice that was significantly larger than the keeper orifice to minimize the impact of the mask on the keeper's operating characteristics. The mask was replaced after each test and the notch was clocked to expose a different segment of the keeper electrode. The mask was held in place by a tantalum sleeve that was spot-welded to the Mo mask and friction fit around the outer diameter of the keeper tube. The tabs of the Ta sleeve that folded over the Mo mask and provided the point of attachment also provided unexposed surfaces on the Mo mask for measurement reference.

Figure 4.—Mo mask on keeper electrode.

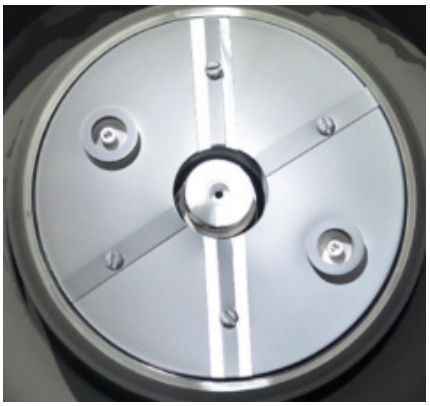

Figure 5.—Mo strips on the IFPC. Note graphite masks on both Mo strips and on IFPC.

2.4.2 Inner Front Pole Covers

As shown in Figure 5, the inner front pole covers (IFPC) incorporated a number of components to characterize their wear. Four polished graphite inner pole covers (IFPCs) incorporated two notches for 1.5 mm thick Mo strips which lay flush with the graphite surface. Two of the pole covers also incorporated two bushings that simulated the fastener attachment configuration proposed for the EDU. The Mo strips were machined flat and had inner and outer radii that matched those of the inner front pole cover. Two 0.5 mm thick graphite masks covered the center third of each of the Mo strips and two similar masks covered graphite radii at 60° clocking. New Mo strips were exposed in each test. Graphite masks were reused test to test.

At the onset of the performance characterization test, only the IFPC used during the TDU-1 wear test (i.e., no polished, Mo-inlaid one) was available. This was deemed sufficient since the wear would be impacted by the large degree of throttling inherent in the characterization test. Graphite masks were incorporated nevertheless to provide reference surfaces. A large fraction of the test segment was conducted as if it were a wear test at 600 V, 12.5 kW, and the wear associated with this one operating condition might be deduced using data obtained from the other wear tests.

Two of the seven tests incorporated “used” IFPCs. The same IFPC was used for both segments of the testing in VF-6 because the tests were separated by sufficient time to allow full mapping of the eroded surface after the first test. The IFPC used during the 500 V test in VF-5 was also used for the last test, the 600 V, 12.5 kW, with increased magnetic field strength (125 percent nominal).

2.4.3 Outer Front Pole Covers

Figure 6 shows one of two 0.5 mm thick Mo surfaces attached to the outer front pole cover (OFPC) in each of the test segments. No OFPC Mo surfaces were present during performance testing. As with the Mo strips on the IFPC, 0.5 mm thick graphite masks covered roughly 1/3 the width of each of the Mo surfaces on the OFPC. The Mo surfaces were attached at the same clocking on the graphite OFPC. This provided an integrated erosion rate over the 1000 h of testing in VF-5 and 500 h in VF-6. The erosion rates observed in 2016 were small enough that no erosion was expected to be detected even with the integrated value. Virgin Mo surfaces were incorporated for each of the tests while the masks were reused.

Graphite pieces were machined to simulate the fastener configuration proposed for the EDU. As with the bushings on the IFPC, these were incorporated to both verify that a non-flat surface would not impact TDU/EDU performance and to identify any erosion that might occur due to radially moving high-energy ions.

Figure 6.—Mo strip on OFPC with graphite mask.

2.5 Measurement of Erosion Profiles

All measurement of erosion depths (and deposition heights) were made using a chromatic, white-light non-contact bench-top profilometer. This is the same technique used to characterize erosion following segments of the 2016 TDU-1 wear testing. The uncertainty in the absolute height measurements depended on both reflectivity of the interrogated surface and its degree of polish. Typically, polished surfaces required less light to achieve a reliable measurement than eroded or coated surfaces. This was particularly true of eroded graphite. However, relative depths of a masked and eroded graphite surface were resolvable within 1 μm. Relative depths of masked and eroded Mo surfaces were resolvable within 5 μm. The difference was due to the roughness of the eroded Mo surfaces. Sources of additional uncertainties are discussed in detail below.

3.0 Results

Results are presented beginning with performance trends, proceeding through erosion data associated with different components, and concluding with plume data. Molybdenum erosion data is presented with the graphite data, but emphasis is placed on the graphite data since they directly represent the erosion of thruster components. At the beginning of the presentation of the erosion data, a more thorough discussion of the uncertainties associated with these measurements is also presented.

3.1 General Observations

No erosion of the BN channel was observed. Deposition indicated by nearly uniform blackening of the channel occurred within the first 100 h of operation in VF-5. Tens of hours of TDU-3 operation in VF-6 prior to the wear testing in VF-5 did not yield significant blackening (Ref. 18). No cracking of the BN was observed at any time. Spalling of carbon deposition on the downstream flats of the channel which was observed after 500 h on TDU-1 in 2016 was not observed on TDU-3 until the thruster was removed from VF-5.

Post-test measurements of the TDU-3 anode showed the thickness of carbon deposition to be on the order of 2 μm, consistent with the QCM measurements. Spalling of the deposition on the anode was observed after every facility opening following TC-2 (i.e., after 500+ h of total operation and 2 prior facility ventings). The spalling was limited to the upper half of the anode and the spalling pattern changed with each entry.

3.2 Performance Trends During Wear Testing

Two sets of performance trends are discussed in relation to the wear test campaign. The first is the repeatability of thruster performance at different operating conditions over the course of the test campaign which speaks to the consistency of the thruster's configuration and adds confidence to the comparison of

wear rates taken during different tests. The second is the consistency of the thruster's operation over the course of individual test segments and allows the comparison of various parameters such as discharge oscillations and background pressure.

3.2.1 Reference Firing Conditions

Six throttle conditions were selected as reference firing conditions (RFCs) to evaluate the consistency of the thruster over the test campaign. Slightly different than the RFC's of previous TDU testing, the conditions correspond to the five wear test operating conditions given in Table I (TC 1-5) with the addition of a 300 V, 3 kW condition. In general, only one set of reference data was collected during each of the short duration wear tests to minimize the operating time spent away from the nominal wear test condition which might add additional uncertainty to the wear data.

Figure 7 shows the variation in power-corrected thruster efficiency as a function of time for the five tests conducted using TDU-3. The slight variations likely result from the data being collected at different points during each short duration test (and thus corresponding to slightly different thermal conditions.

There were no significant variations in peak-to-peak values of discharge current, J_d, and discharge voltage, V_d, over the course of the testing. (Typical values are given in Table I.)

As noted in Table I, the keeper electrode floated roughly 2 V above cathode potential during thruster operation for all operating conditions. Figure 8 shows the variation in peak-to-peak values of the keeper voltage with respect to the cathode as a function of thruster operating time. Note that the highest values are for TC-3, and TC-5. The lowest values are for TC-2. The peak-to-peak trends in V_k were also observed in the peak-to-peak values of the cathode to ground voltage, V_{cg}. However, the values of the latter were roughly twice that of former. The peak-to-peak values of V_k and V_{cg} are determined and constrained by the cathode-tied configuration. The body current runs from the plasma to all surfaces exposed to the plasma except the anode, discharge channel, and keeper through the cathode back to the plasma.

Discharge current was maintained by operator-adjustment of the flow rates. The discharge current varied by as much as 0.1 A (0.5 percent) due to flow adjustments, noise in the anode flow controller, and thermal variations as the TDUs reached steady state. Significant variation in both J_d and V_d occurred during performance characterization testing (165 to 350 h), but note that the majority of TDU-3's operation during this segment was at 600 V, 20.8 A. Roughly 3.5 percent of the nominally 300 V, 6.3 kW test in VF-6 operated at 600 V to accommodate thrust vector analysis. With the exception of the performance characterization segment, the vast amount of operating time was spent at the nominal wear test condition and erosion profiles are assumed to be independent of the slight periods of deviation.

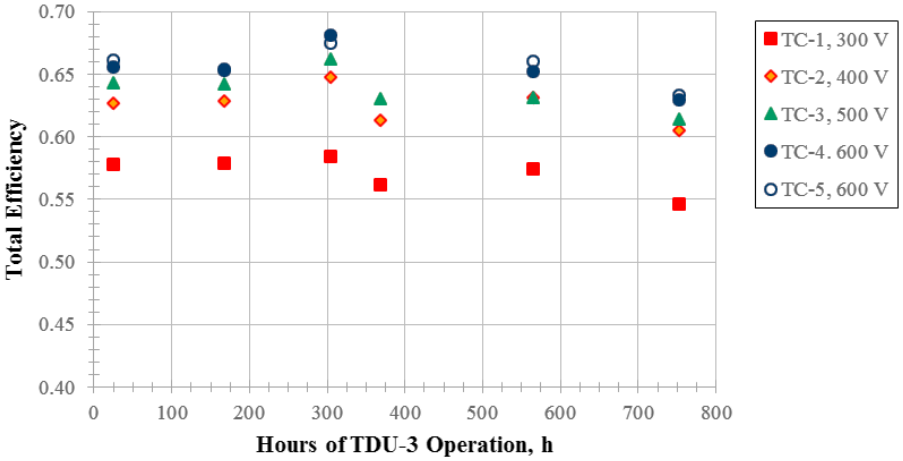

Figure 7.—TDU-3 total efficiency as a function of time during wear testing.

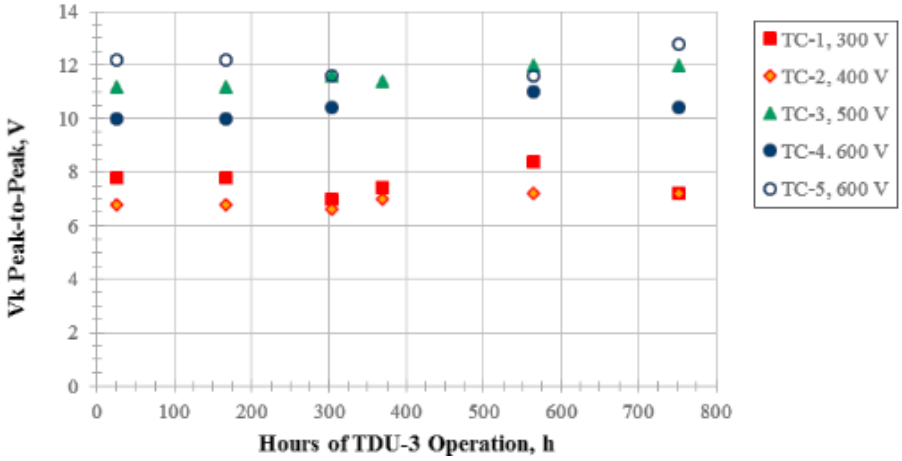

Figure 8.—TDU-3 keeper voltage (peak-to-peak values) as a function of time during wear testing.

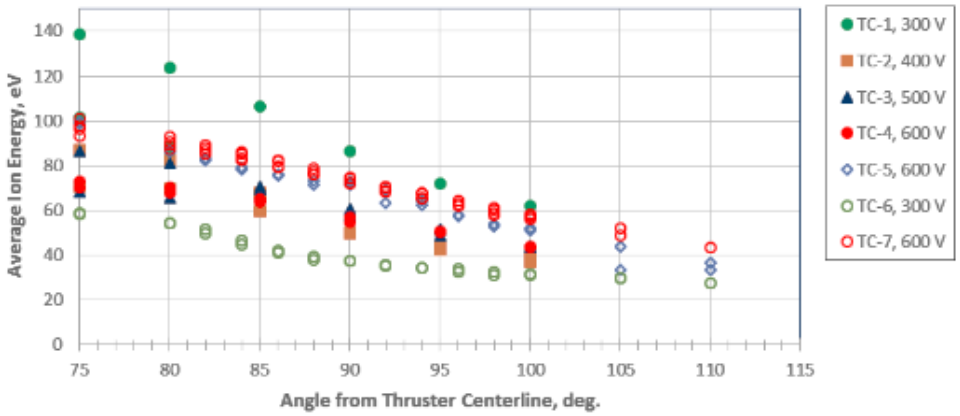

Figure 9.—Average ion energy in the wings of the plume of both TDU-1 and TDU-3 during wear testing.

Plume data consisting of Faraday probe, Langmuir probe, retarding potential analyzer (RPA) probe, and Wein filter (ExB probe) were collected 1.5 m from the thruster exit plane in an arc ±115° from thruster centerline. Data were collected during each short duration wear test and during TDU-3 performance testing. Detailed discussion of this data is not included in this paper, but trends in the wings which could be correlated to the trends in erosion are presented. Figure 9 compares the average energy in the plume as a function of angle from centerline. While the fluxes in the wings are small, Figure 9 shows that a significant fraction of the ions have energies above 60 eV, especially for cases TC-1, TC-5 and TC-7. In contrast, TC-6 appears to have the least energetic ions in the wings of the plume.

3.3 Uncertainties in the Erosion Measurements

In addition to the resolving capabilities of the profilometer discussed above, there are several other sources of uncertainty in the erosion measurements. As noted above, the uncertainties lie principally in the measured depths (μm) and not in the rates themselves. The time of each wear test segment was known within a fraction of an hour, or within less than 0.5 percent which would correspond typically to a graphite erosion depth of 0.04 μm, far less than the actual measurement uncertainties noted above and in what follows. The actual uncertainties in the measured erosion rates then decrease with eroded depth (i.e.,

are less with greater erosion rates) and with longer test times (i.e., the measurement errors are not compounded by extrapolation to 1000 h).

Carbon (and a small amount of stainless steel) was sputtered on the TDU surfaces from plume impingement onto facility walls at a rate of 2 μm/kh onto TDU-3 in VF-5 and 0.5 μm/kh onto TDU-1 in VF-6. For an average test duration of 200 h, this amounts to a possible direct change in surface height of about 0.4 μm which is below the detection threshold of the profilometer (and well within the measured surface roughness). The impact of carbon deposition on graphite erosion is assumed to be at worst additive (i.e., 1 μm of deposition would cancel 1 μm of erosion). However, the impact of carbon deposition on Mo surface erosion rates has been shown to be more complicated resulting in the onset of no net erosion below a critical impingement current density for a given xenon ion energy (Ref. 20). The measured Mo erosion rates appear to be of such high values on the IFPC that this effect can be neglected.

The masked and eroded surfaces were compared within a few mm of each other to minimize the impact of surface variations resulting from pre-test polishing and mounting in the profilometer apparatus. Both of these introduced further uncertainty if the surface was numerically flattened in post-processing of the profilometer data. The impact of surface variations was minimized by comparing data taken on both sides of a masked region and on multiple masked regions (usually 180° apart). No azimuthal variation in wear of the graphite IFPC was observed in the 1700 h wear test (Ref. 9), which suggests the azimuthal uncertainty is less than 0.6 μm/kh. Variations across the surface or within 1 mm of a measured region introduced an average of 0.5 μm of uncertainty (±0.25 μm) in the graphite erosion rate calculations and up to 5 μm of uncertainty in the Mo erosion rate calculations. Remeasuring of eroded surfaces, both Mo and graphite, yielded nearly identical results, suggesting that there were not additional systematic errors.

Recalling that the measurement resolution uncertainty is 1.0 μm (±0.5 μm) the error in graphite erosion depth is roughly ±1.2 μm which corresponds to ±6.0 μm/kh for a 200 h test extrapolated to 1000 h. Figure 10 compares the graphite erosion rates measured on the IFPC of TDU-1 during two segments of the 1700 h wear test in 2016 (Ref. 9). Note that the rates of the shorter duration have much larger uncertainties, but that the uncertainties are not sufficient to account for the difference in the rates measured in the two segments. The potential of a much larger source of uncertainty, initial rates versus sustained rates, is discussed in Section 4.0 and is shown to not explain the differences in the two trends in Figure 10.

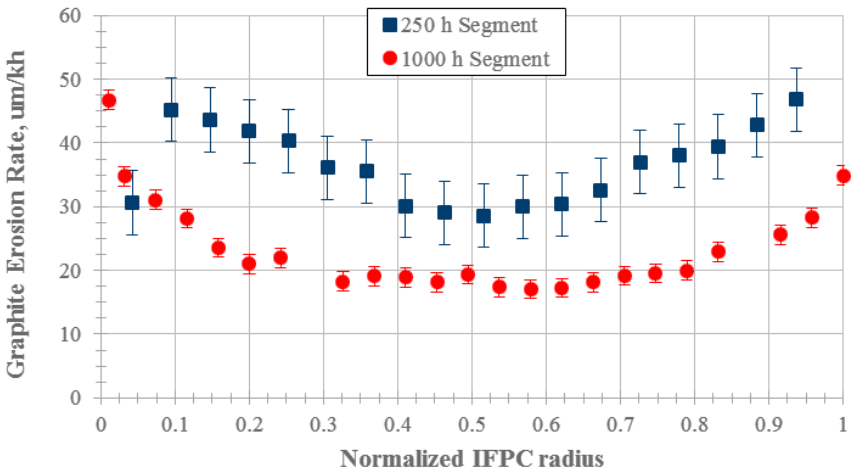

Figure 10.—Graphite erosion rates of the TDU-1 IFPC for two segments of the 2016 1700 h wear test (Ref. 9).

Additional uncertainty arose in the measurement of eroded depths of Mo surfaces. The graphite masks on the Mo strips caused the strips to erode non-uniformly. Modifications to the masking including reducing the mask width and testing without masking show that depths near the edges of the strips were most representative of unmasked Mo erosion. There appears to be a correlation of the Mo erosion to the ExB drift of the near-field plasma. However, this effect has not been fully characterized. Also, there was unequal erosion on either side of the radial mask. Together, these introduced a relatively consistent 10 percent uncertainty in the eroded depth. Since the resolution uncertainty for Mo erosion measurements is ±2.5 μm, the overall measurement uncertainty for the Mo depths is ±5.0 μm which corresponds to ±25 μm/kh for a 200 h test extrapolated to 1000 h. Since the measured Mo depths were typically much larger than this, the relative uncertainty in the Mo data was taken to be ±10 percent.

3.4 Keeper Erosion

The keeper electrode in TDU-3 exhibited unexpectedly high levels of erosion. Figure 11 shows an image of the keeper post test formed by profilometer measurements and indicates which region corresponds to a particular segment of the testing. Note that there is a circular step forming an annulus around the inner aperture which was unmasked throughout the test campaign. This is a region of erosion roughly 50 μm deep and represents aggregate erosion over the 996 h of TDU-3 operation. An isometric image of the keeper face is given in Figure 12 and shows the relative depth of the different regions.

Figure 13 shows a profilometer image of the keeper face from TDU-1 which can be contrasted with that in Figure 12. Unlike the raised, reference regions in Figure 12 which correspond to protected segments of the TDU-3 keeper, the raised region in Figure 13 is the exposed region—showing net deposition. Note that the exposed segment was exposed for both wear tests in VF-6 in order to resolve the expected low erosion rates (measured on the keeper of TDU-1 in 2016 after 1700 h). The exposed regions (cutout and inner annulus) show net deposition of 15 and 8 μm, respectively (with no discernable radial variation). These correspond to deposition rates of 60 and 24 μm/kh, 50 to 100 times greater than the QCM-measured deposition rates from the facility. High-resolution imaging of the deposition shows the deposited graphite to be columnar and covering only ~ 30 percent of the Mo surface. This is radically different from the deposition observed on the QCM crystals and on the OFPC of TDU-1 which was densely packed (Ref. 9). The difference in the morphology of the deposited graphite is likely due to the dense plasma near the keeper orifice.

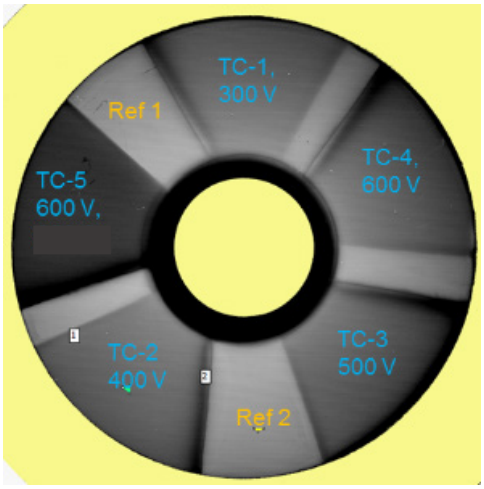

Figure 11.—Regions of TDU-3 keeper exposed during each of the short duration wear tests in VF-5.

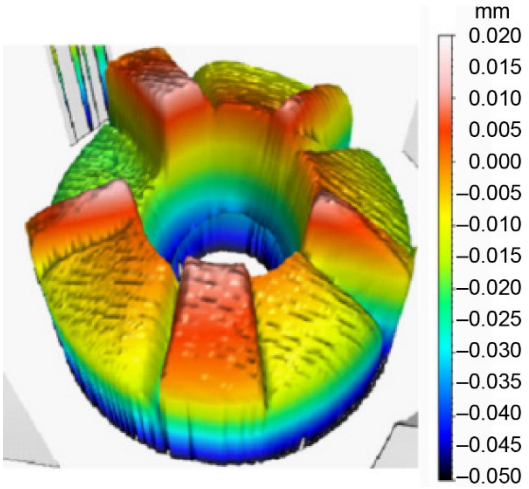

Figure 12.—Erosion of the TDU-3 keeper during each of the short duration wear tests in VF-5.

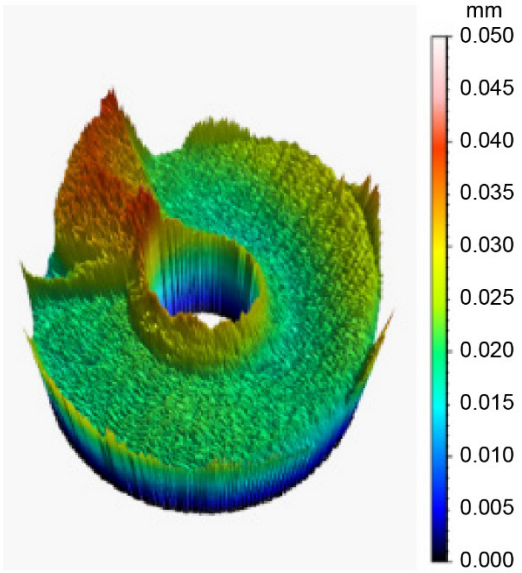

Figure 13.—Deposition on the TDU-1 keeper following the two short duration wear tests in VF-6.

Figure 14.—Comparison of Mo keeper masks for TDU-1 and TDU-3 for similar operating conditions.

Figure 14 compares photos of the Mo keeper masks of the 300 V TDU-1 and TDU-3 short duration wear tests (TC-6 and TC-1, respectively). Note the net deposition (~ 8 μm thick) around the center of the TDU-1 mask. Slight erosion was observed beyond the region of deposition on the TDU-1 mask with rates roughly 10 percent that of the TDU-3 mask. The four tabs visible in each of the pictures correspond to the attachment points for the Ta collar that held the mask onto the keeper. The surfaces protected by the tabs also provided zero-erosion, zero-deposition surfaces for wear measurements.

Figure 15 compares the erosion profiles of each exposed section of TDU-3's keeper with respect to the two "reference" sections (see Figure 11). Note that the high-magnetic field case (TC-5) has a significantly different erosion pattern. Except for the extreme outer radius, the rates for the other test conditions follow the same trends and nearly lay within the uncertainty of the measurement. The depth of the step at the inner radius of the TDU-3 keeper is 50 μm which corresponds to a time-weighted linear addition of the rates observed at the inner edges of the segments which were each exposed for only one of the tests. This implies there was no significant change in erosion rate over time and that the polished surface of the keeper did not accelerate the erosion observed in each segment.

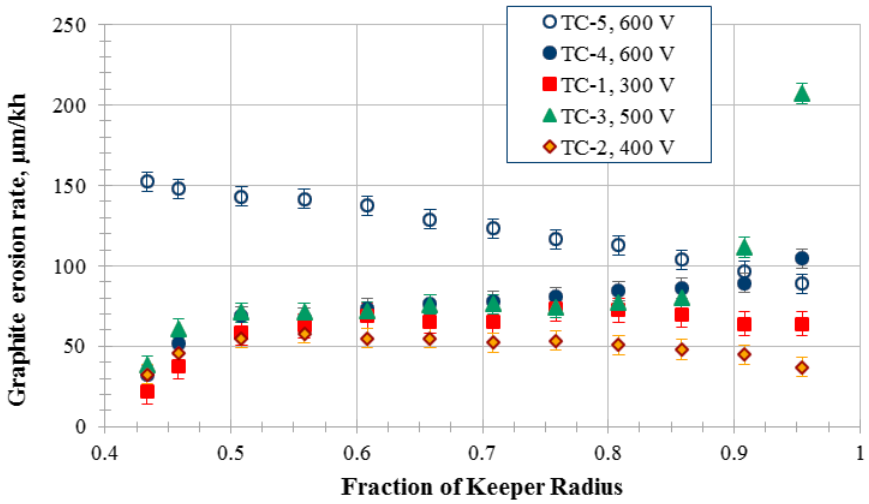

Figure 15.—Erosion rates of the TDU-3 keeper as a function of keeper radius each of the short duration wear tests in VF-5.

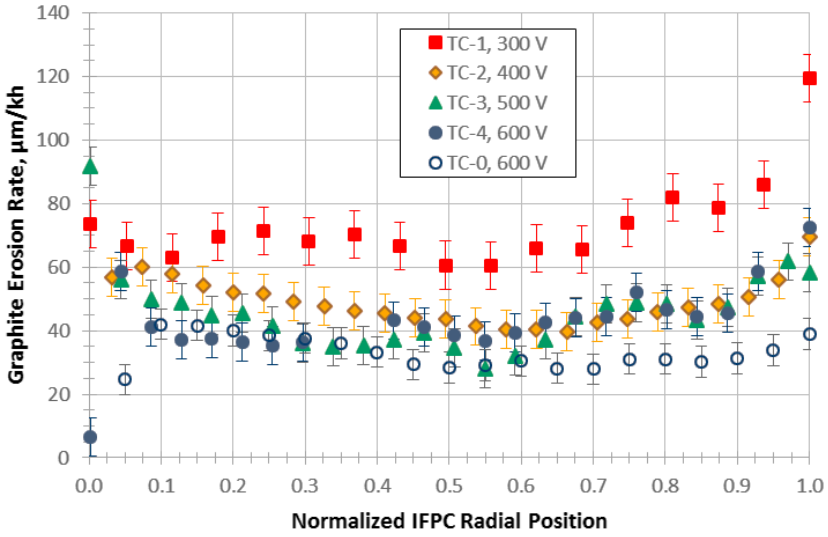

Figure 16.—Comparison of IFPC erosion as a function of discharge voltage.

3.5 Inner Front Pole Cover Erosion

The erosion of the inner front pole cover of TDU-3 as a function of discharge voltage is shown in Figure 16. All data is for the thruster being operated with the nominal magnetic field. For reference, the 250 h erosion pattern of TDU-1 (TC-0) is also shown. Error bars indicate that there is very little variation in erosion rates except for the 300 V data, which is between 50 and 100 percent greater than those for other discharge voltages. Exceptions to this rule occur at the extreme inner and outer radii. For comparison, the erosion rates measured following the performance characterization test (TC-4) are included. Figure 17 shows that the erosion trends of the Mo strips followed the same general trends as the graphite IFPC, though the rates, as discussed in detail below, were much higher, especially near the inner radius of the IFPC.

Figure 18 shows that operating at a higher magnetic field had minimal impact on the IFPC (graphite) erosion rates except at the extreme inner radius. This is in clear contrast to the erosion rates of the Mo strips with nearly 20 times greater near the inner radius as shown in Figure 19. (Note that no Mo data were collected for TC-4.) The higher graphite erosion rate for TC-5 at the inner radius of the IFPC

contrasts with the dip seen in the TC-0 and TC-4. This may correlate with the higher erosion measured on the keeper which was much greater for this (TC-5) condition.

Figure 20 shows that there is a clear, but inconsistent, impact of pressure on IFPC erosion rates. As noted in Table I, TC-0 corresponds to TDU-1 operation in VF-5, TCs 1-5 correspond to TDU-3 operation in VF-5, and TCs 6-7 correspond to TDU-1 operation in VF-6. However, performance variations were negligible for operation at the same discharge voltage and power regardless of TDU or facility. Therefore, the significant changes are believed to be dominated by the change in facility pressures. The erosion rate of the 600 V case is much higher at higher pressure (TC-7 vs. TC-0 and TC-4) whereas the erosion rate of the 300 V case is significantly lower (TC-6 vs. TC-1) at higher pressure. However, the trends observed on Mo strips show consistently decreasing erosion rates with pressure. Figure 21 compares data for 600 V, 12.5 kW operation in several test campaigns over a range of pressures. The SLA data suggest a varied trend, with outliers on both the inner and outer IFPC radii (Ref. 11).

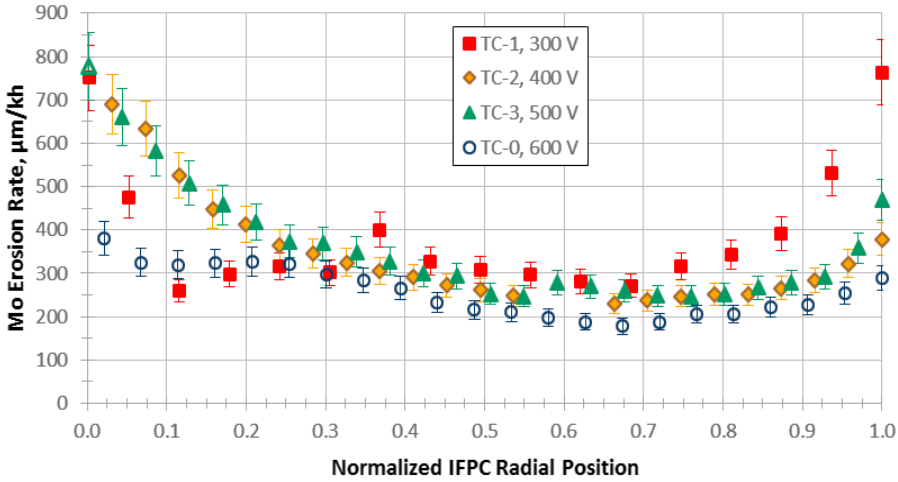

Figure 17.—Comparison of Mo strip erosion across the radius of the IFPC.

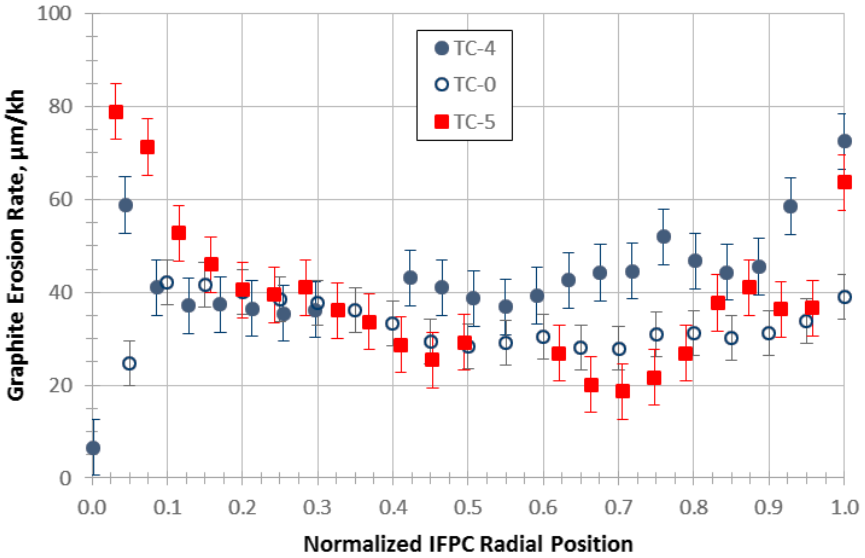

Figure 18.—Comparison of IFPC erosion as a function of magnetic field for V_d = 600 V in VF-5. Note that TC-5 has a 125 percent higher B-field.

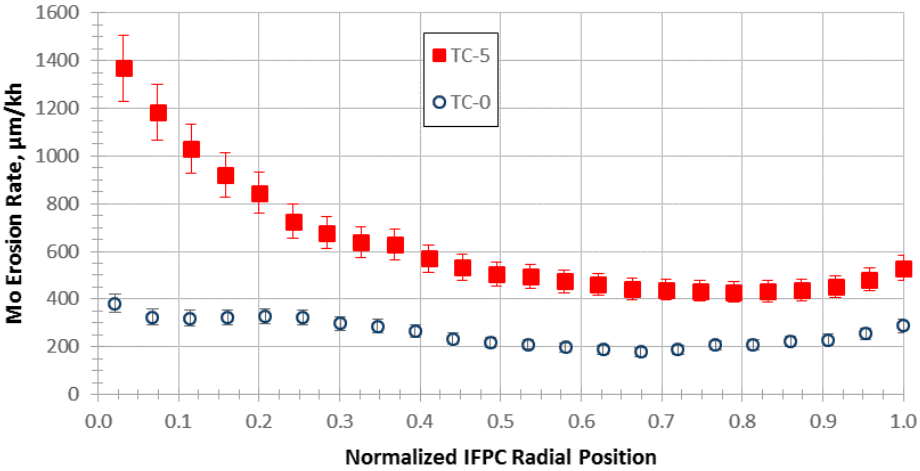

Figure 19.—Comparison of IFPC Mo strip erosion as a function of magnetic field for V_d = 600 V in VF-5. Note that TC-5 has a 125 percent higher B-field.

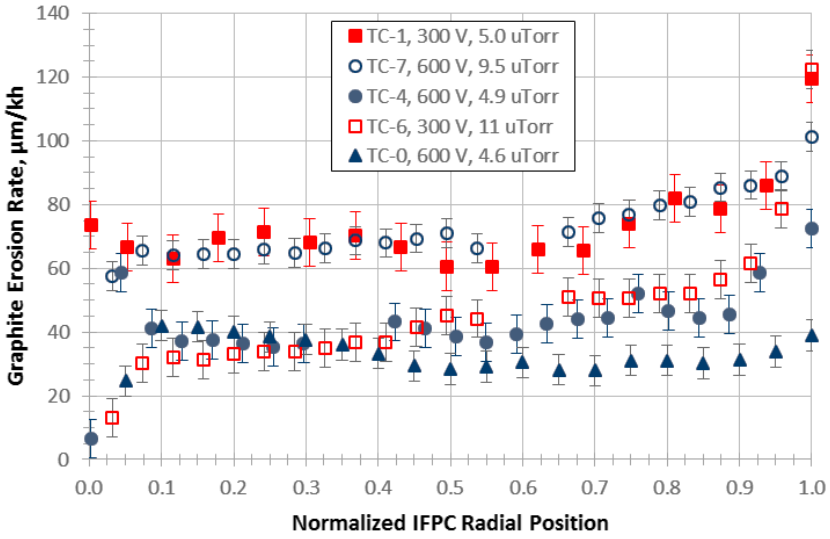

Figure 20.—Comparison of IFPC erosion as a function of facility pressure.

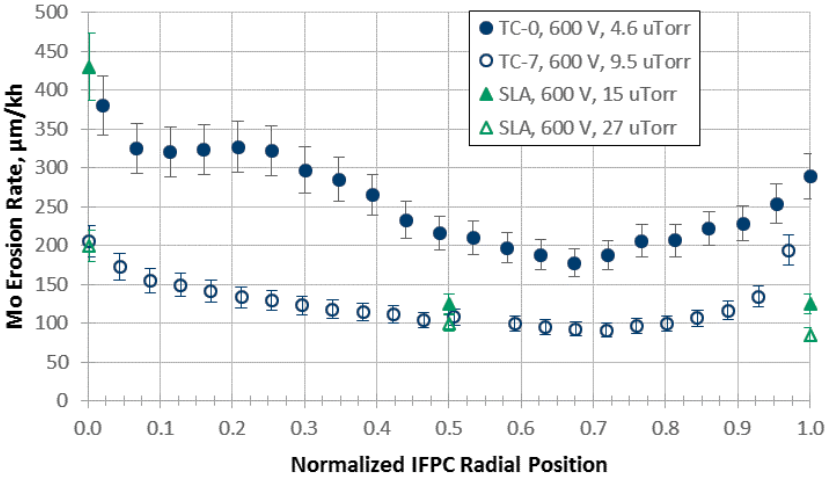

Figure 21.—Comparison of Mo erosion as a function of facility pressure.

3.6 Outer Front Pole Cover Erosion

No erosion was measured on the outer front pole cover (OFPC) of TDU-1 during the 2016 wear testing. No deposition was measured on it either, suggesting a nearly unchanged surface. This was true for both graphite and alumina outer pole covers (Ref. 9). Erosion of the outer pole cover was measured following the completion of the TDU-3 wear testing (after 996 h). Figure 22 shows that the OFPC eroded at a rate between 2 and 10 μm/kh, with (slightly) greater erosion occurring on the inner channel-side of the OFPC.

Figure 23 shows the erosion rates measured on the Mo strip on the OFPC for TC-1, 2, 5, and 7 wear tests. These indicate that the erosion of the graphite OFPC varied with thruster operating condition and that the slightly greater erosion on the inner third of the OFPC (Figure 22) occurred during the 300 V operation. Small Mo erosion rates were observed on the Mo strips for the 600 V operating cases (TC-5 and TC-7; no Mo strips were incorporated for TC-4). Comparing to IFPC and keeper erosion rates, these low Mo rates would likely result in very small graphite erosion consistent with Figure 22 and the results of the 1700 h wear test (Ref. 9).

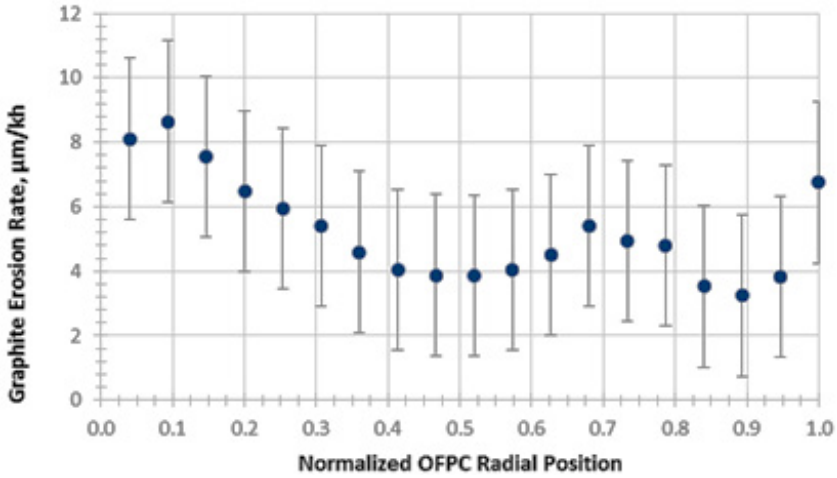

Figure 22.—OFPC erosion as a function normalized OFPC radius.

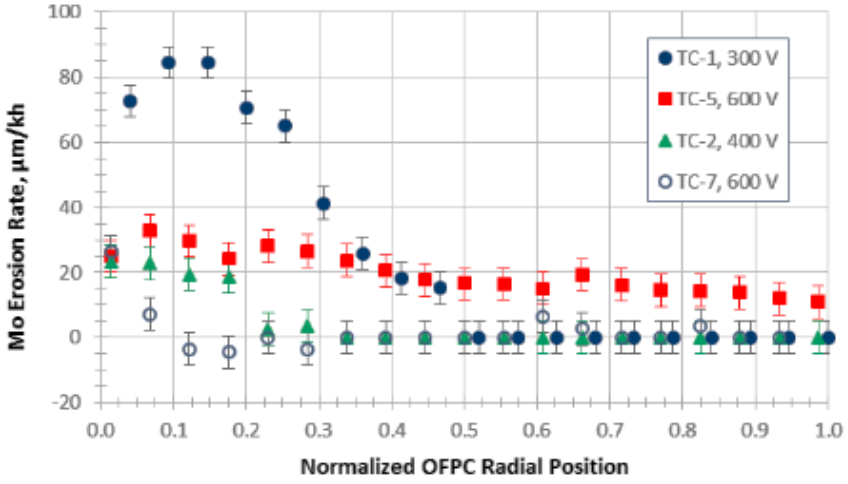

Figure 23.—OFPC Mo strip erosion as a function normalized OFPC radius for several test conditions.

Because the Mo erosion rates vary with operating condition, it's is difficult to draw a conclusion from the ratio of the Mo rates to the aggregate graphite OFPC rates. However, as can be seen in Figure 6, there is shadowing of the OFPC (or its masks) by the fasteners. The "shadowed region" appears as a wake on the far right-hand-side of the image, extending from the fastener to the outer edge of the mask in the figure. Post-test analysis showed the shadowed region consists of back-sputtered material from the facility—indicating that this small area is shielded from "cleansing ions" impinging the OFPC at relatively large angles from normal (Ref. 9). There were no visual differences in the shape of the protected region over all TCs. Similarly, the thicknesses of the films on the protected regions were beneath the detection threshold of the profilometer.

4.0 Discussion

4.1 Trends in Erosion Rates

Table II summarizes the erosion rates observed on the keeper and pole covers for the various TCs presented above. Actual component, i.e., graphite, rates are given for the keeper and IFPC. However, since there were no test-to-test measurements of OFPC erosion, rates calculated for the Mo strips on the OFPC are given. The rates can be cross-referenced to the TDU performance parameters given in Table I.

Maximum and typical values for the graphite erosion rates observed on the keeper are given. For TC-0, the erosion rate was ambiguous and may have been deposition. Deposition was seen in both TC-6 and TC-7, but there was no measurement at the end of TC-7 (which preceded TC-6). Deposition was measured on the Mo masks for each test and showed the deposition rates were comparable. Thus, all three of the TDU-1 tests showed negligible wear of or deposition on the keeper. The five TDU-3 tests showed significant erosion of the keeper, especially for higher magnetic fields. While the erosion of the keeper in the TDU-3 configuration was unexpected, the trends of the TDU-1 keeper erosion were consistent both with expectations and prior wear test data. It is likely that operating with the keeper in the TDU-1 configuration is sufficient to eliminate keeper erosion as a primary failure mechanism without impacting thruster performance.

Inner pole cover erosion, identified as one of the primary AEPS failure mechanisms, appears to have a weak dependence on discharge voltage except near the cathode (inner IFPC radius). However, as seen in Table II, the highest erosion occurred near the channel (outer IFPC radius) for TC-1, 300 V operation which also had the highest overall beam divergence and highest flux of higher-energy ions in the wings of the plume. Similar erosion rates were seen near the channel for TC-6, 300 V operation suggesting the

TABLE II.—SUMMARY OF EROSION RATES MEASURED DURING TDU TESTING

TC	TDU	VF	V_{cg}^{p-p}, V	Magnetic field	Keeper, µm/kh		IFPC, µm/kh			OFPC, Mo µm/kh
					Maximum	Typical	Inner	Mid-R	Outer	
0, 600 V	1	5	28	Nominal	≤10	----	25	25	40	---
1, 300 V	3	5	14	Nominal	75	75	75	60	120	85
2, 400 V	3	5	15	Nominal	55	50	55	40	70	25
3, 500 V	3	5	27	Nominal	210	75	90	30	60	40
4, 600 V	3	5	28	Nominal	110	80	35	40	70	15
5, 600 V	3	5	35	125% Nom	150	125	80	30	65	35
6, 300 V	1	6	14	Nominal	≤20 depo	----	15	40	120	50
7, 600 V	1	6	28	Nominal	≤20 depo	----	55	70	100	20

erosion in this region is coupled to the discharge. The variation in erosion rates for inner radius of the IFPC does not correlate well with TDU, VF, V_d (given in the TC), magnetic field or V_{cg}(peak-to-peak) values. With the exception of TC-4, 600 V, the typical keeper erosion rates do trend with the inner IFPC rates which may suggest that the two are being eroded by the same flux of ions. Significant higher Mo erosion rates near the inner radius of the IFPC (Figure 17) are also comparable to the Mo rates on the outer radius of the keeper masks. Note, however, that the erosion rates near the mid-radius of the IFPC are largely insensitive to TC, with the exceptions of TC-1, 300 V and TC-7, 600 V which are roughly double the other values.

Indeed, as mentioned above, the (graphite) IFPC erosion rates measured for the TC-7, 600 V operation are completely inconsistent with all other data. Remarkable agreement with TC-1, 300 V except at the inner IFPC radius appears to be purely coincidental. The most probable explanation for the inconsistency is a loss in configuration control that led to an artificially high measurement of graphite erosion for TC-7, but this explanation has been eliminated through test documentation. It should be noted, per Figure 9, that the beam divergence of the TC-7, 600 V case is most comparable to the TC-1, 300 V case. This does not resolve the disconnect between the trends in Mo data or the comparison of Mo to graphite rates discussed below. It does, however, suggest that the graphite data are not completely spurious.

The common unexpected trend of the wear testing of TDU-1 and TDU-3 is that the first wear test of each thruster in a given test series (TC-0 and TC-1 in VF-5 and TC-7 in VF-6) resulted in graphite erosion rates twice that experienced in other tests. One is tempted to infer that polished pole covers or other beginning-of-test conditions yield significantly higher IFPC rates. If true, the results would be modified in ways that are desirable from both perspectives of thruster development and fundamental understanding of thruster erosion processes:

- The change in TDU-1's pole cover erosion rates in 2016 would be explained and the lower, later rate would be representative of future tests,
- There would remain no significant variation in graphite pole cover erosion with either discharge voltage or facility pressure
- The erosion of the IFPC during TC-5, higher magnetic field operation would be scaled higher, to compare with the erosion observed on the keeper.
- The keeper erosion rates would all be reduced by the same rough factor of two since each segment began as a polished surface.

However, there is no justification for this conclusion. In particular, the unpolished, well-worn IFPC incorporated during the performance characterization testing yielded the same erosion rates as the other, polished IFPCs; and the polished surfaces of the TDU-1 250 h segment (TC-0, 600 V in Table I and Table II) which were exposed during the 1000 h, fourth segment of the 1700 h test eroded at the same, reduced rate as the previously exposed surfaces. The TC-7, 600 V case operated for only a short duration (< 24 h) before an opening of VF-6 was required. The polish had been removed from the surface after this short duration and the IFPC masks were adjusted which captured a small fraction of the partially eroded surface under a mask. The erosion depth was undetectable via profilometry, only the change in surface quality was measured. In addition, it should be noted that the increase in IFPC erosion with pressure is noted between two polished IFPCs operating at 600 V (TC-0 and TC-7), not just between the 300 V and 600 V cases with the same IFPC. Therefore, the unexpected trends cannot be dismissed simply on the basis of whether the IFPC erosion initiated on a polished, untested surface.

TC-0, TC-1, and TC-7 were initiated with different amounts of back-sputtered material on the BN channel. TDU-1 (TC-7) retained the well-coated BN channel from the 1700 h test. While TC-1 (TDU-3) testing did begin with a relatively clean channel, TC-0 (TDU-1) began after a 125 h of performance testing and the channel was, as for TC-7, well-coated (Ref. 9). Moreover, there appears to be no physical path to increasing the graphite erosion while simultaneously decreasing the collocated Mo erosion. As seen above and in the discussion below correlating Mo to graphite regression rates, TC-7's graphite erosion is out of family with all of the other operating conditions. No explanation is apparent at this time, but the IFPC erosion rates for TC-7 must be considered highly suspect.

To some extent, the erosion rates of the Mo strips on the OFPC correlate with the ion fluxes in Figure 9. However, since the erosion rates appear to maximize near the channel (the inner radius of the OFPC), it is more probable that the rates in Table II correlate to the position of the ion acceleration zone. TC-2, 400 V data do not fit into this trend.

4.2 Correlation of Molybdenum and Graphite Erosion Rates

Because of the differences in yields, the erosion rates of the Mo on the keeper, IFPC, and OFPC are of most value when correlated with the rates and trends of the erosion of the graphite components themselves. The correlation may provide insight into the energies (and thereby source) of the eroding ions and the variation of ion flux with operating condition and location.

An extensive assessment of the sputter yields of Mo and carbon, C, surfaces has been undertaken by Yim (Ref. 21). Leveraging the conclusions of this analysis which are subject to high uncertainties, a preliminary assessment of the ion flux to the IFPC has been undertaken. Figure 24 shows the volumetric sputter yields of Mo to C as a function of incident ion energies for normal-incident Xe II ions. Volumetric sputter yields are of more value to this analysis than typical sputter yields in units of atoms per ion since the ratio of volumetric yields can be correlated to the ratio of regression (erosion) rates as are reported above. Figure 25 shows the ratios of the yields, for various angles of incidence. Note that the values for 0° and 15° overlap and that the impact of angle of incidence is largely independent of ion energy, yielding a consistent reduction from the value of the ratio at normal (0°) incidence. Near the threshold energy of C sputtering, the ratio increases rapidly. Due to the uncertainties in the erosion rate measurements, Figure 25 does not provide sufficient information to draw quantitative conclusions regarding the ions eroding the TDU surfaces (Ref. 21). However, the relative significance of ion energy and angle of incidence may be sufficient to draw some qualitative conclusions. This is further complicated by the nature of graphite erosion due to low-energy ions as it is dominated by dimer and trimer removal (Ref. 22).

Figure 26 compares the ratio of TDU-3 IFPC Mo to C (graphite) erosion rates as a function of discharge voltage. Uncertainties have been increased reflecting the uncertainties associated with both Mo and C rates themselves. For TC-1, TC-2, and TC-3 data, the ratios are similar over the majority of the IFPC radius between values of 5 and 8. From Figure 25, this suggests incident ion angles above 45°, with no resolution of the ion energies themselves. However, protrusions on the IFPC including fastener heads, graphite masks, and bushings for the fasteners did not reveal any shadowed regions as were seen on the OFPC (Figure 6). Detailed profilometry near an IFPC bushing for TC-2, TC-3, and TC-5 showed masking where the bushing overlapped the IFPC but otherwise, in 360°, erosion consistent with the rest of the IFPC. This suggests the eroding ions were nearly normal in incidence. Unless the ions were in the high-energy tail of a high-temperature (many eV) distribution with a hundreds of eV mean energy, there is no corresponding region in Figure 25 that would have normally incident ions with that ratio of yields. If, however, the curves are overestimating the ratio values, then there would be two populations of ions that could result in the erosion, low-energy (sub 100 eV) and high-energy. Without further measurement, it is impossible to determine which population is dominant. However, the overlap of the curves suggest the same source and energy of ions are responsible for the IFPC erosion for TC-1, TC-2, and TC-3 (300 V to 500 V operation).

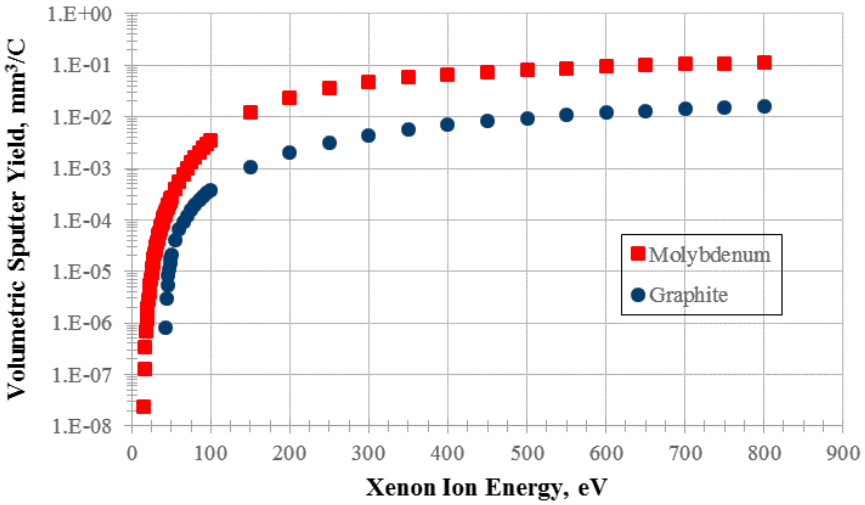

Figure 24.—Mo to C volumetric sputter yields as a function of normal-incident Xe II ion energies (Ref. 21).

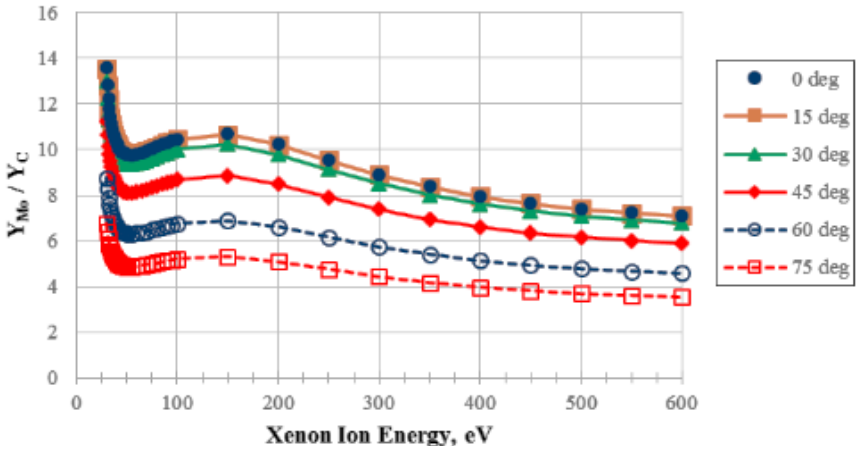

Figure 25.—Ratios of Mo to C volumetric sputter yields as a function of incident Xe II ion energies.

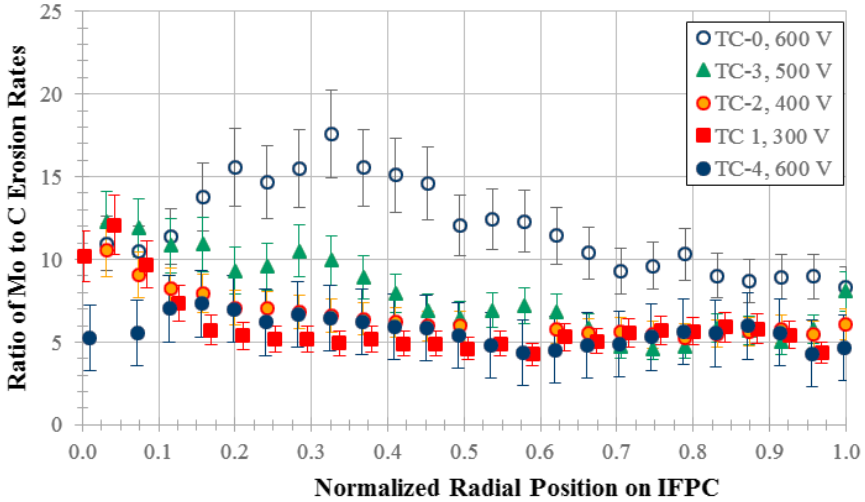

Figure 26.—Ratios of Mo to C IFPC erosion rates as a function of discharge voltage.

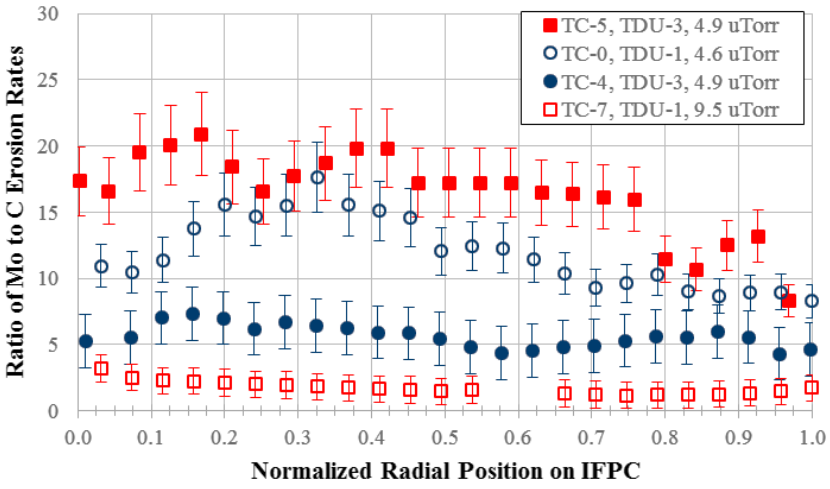

Figure 27.—Ratios of Mo to C IFPC erosion rates as a function of facility pressure and TDU configuration for V_d = 600 V.

Since there was no dedicated 600 V, 20.83 A test using TDU-3, assessing whether this operating condition falls along the same trends is problematic. The ratio for TC-0 (TDU-1) is shown in Figure 26. Note that it has a fundamentally different trend. This may result from either the configuration differences between TDU-1 and TDU-3. A ratio of the graphite erosion observed during TC-4, 600 V and Mo erosion from TC-0, 600 V is also shown in Figure 26. Note that the ratio now trends with the other TC's except near the IFPC's inner radius. The difference in Mo erosion rate near the cathode very likely follows from the differences in TDU-1 and TDU-3 cathode location. The convergence of the TC-4 data with the other data over the rest of the radius suggests that there is a fundamental difference in IFPC erosion between the two configurations. Unfortunately, TC-7, 600 V ratios trend differently from both TC-0 and TC-4 data as shown in Figure 27. Lower graphite erosion relative to Mo erosion shown in Figure 16, Figure 17, and Figure 26 suggest TDU-1's IFPC was eroded by lower0energy ions (regardless of angle of incidence) than TDU-3's IFPC.

Figure 27 compares all four sets of 600 V data (TC-0, 4, 5, and 7). TC-5's higher magnetic field significantly increases the ratio of Mo to graphite erosion without significantly changing the graphite erosion rate itself (cf. Figure 18). Indeed, the graphite erosion rates of TC-0, 4, and 5 are comparable except near the cathode. The variation in the ratios shown in Figure 27 indicate that there are more low-energy ions near the cathode (inner radius of the IFPC) for the higher magnetic field of TC-5. The increase in low-energy ions is also consistent with the ratio of regression rates shown in Figure 25, where values above 15 would likely lie in an extrapolation (within the uncertainty) near the threshold region of the curves. Again extrapolating within the uncertainties in Figure 25, the very low values of TC-7 in Figure 27 would suggest that the IFPC erosion is dominated by high-angle of incidence ions at higher pressures. This is consistent with some previous investigations (Refs. 10 and 13). Unfortunately, regardless of whether this explanation is valid, the TC-7 data do not support a conclusion regarding differences in the IFPC erosion of the two TDU configurations since the Mo rates trend in the opposite direction.

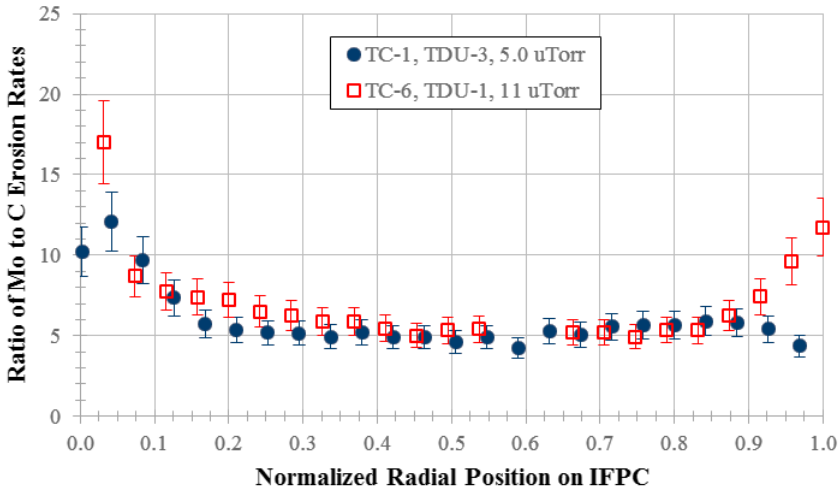

Figure 28.—Ratios of Mo to C IFPC erosion rates as a function of facility pressure and TDU configuration for V_d = 300 V.

Figure 28 compares the ratios of Mo to graphite (C) erosion rates for the two 300 V test conditions, TC-1 and TC-6. Recall from Figure 20 that the rates of graphite erosion of TC-6 are roughly 50 percent of those of TC-1. That the two sets of data in Figure 28 lie on nearly on top of each other over the majority of the IFPC radius suggests that the reduction in erosion associated with the higher background pressure is due to a reduction in overall flux of eroding ions and independent of a change in angle of incidence or mean energy. However, there could have been a proportional change in both that yielded the same values, but that is less likely. The differences in the ratios in Figure 28 near the outer radius suggest differences in the fluxes of low-energy ions.

That 300 V and 600 V erosion patterns vary differently as the pressure increases suggests that there is a fundamental difference in the plasma structure. This is consistent with both the plume data shown in Figure 9 and previous investigations (Refs. 6, 7, and 15). It is unclear, however, what role the TDU configuration played and whether the plasma differences would be expected to yield the changes in erosion trends.

4.3 Implications of the Erosion Rate Measurements

The TDU-1 cathode location yielded negligible keeper erosion in both high and low-pressure tests at 600 V (TC-0 and TC-7) and for 300 V at elevated pressure (TC-6). However, it remains undetermined if a higher magnetic field will result in keeper erosion also in the TDU-1 cathode configuration. The TDU-1 location is to be preferred over the TDU-3 location as the keeper erosion is likely to be negligible for nominal magnetic field operation.

Inner front pole cover erosion was shown to be relatively insensitive to discharge voltage which was the primary throttling mechanism for the AEPS missions (Refs. 4 and 5). Erosion near the discharge channel did decrease with increasing discharge voltage. This is consistent with the lower discharge voltage having higher energy ions in the plume at high-angles from normal to the surface. While a higher-than-nominal magnetic field was shown to have a substantial impact on keeper erosion, there was only minimal impact on the erosion of the IFPC. Outer front pole cover erosion appears negligible for all operating conditions.

Facility pressure appears to have a significant impact on the measured erosion rates. However, the trend in graphite erosion rates is inconsistent both with themselves and with the trends in Mo erosion rates

for different discharge voltages. The 600 V (TC-7) case in VF-6 has several inconsistencies including comparable Mo and graphite erosion rates and significantly increased erosion with pressure whereas Mo rates decreased. Consensus of the test team is that the trend of decreasing IFPC erosion with facility pressure is accurate. This was seen with all Mo TDU-1 and TDU-3 data, 300 V graphite TDU-1 and TDU-3 data, and (less clearly) Mo TDU-2 data. (The TC-7 graphite erosion rates remain a topic for ongoing review.) Regardless, the data do suggest that wear rates should be evaluated in the lowest pressure environment possible.

Ratios of the Mo to graphite erosion rates of the IFPC may prove helpful in refining numerical models of the eroding processes. However, the trends shown in the Mo data appear to not represent those seen in graphite data because of Mo's higher sensitivity to low-energy ions. Trends which do appear to be captured by Mo-only data are the relative insensitivity to IFPC erosion at mid-radius, an increase in inner-radius IFPC erosion with higher magnetic field, and a decrease in IFPC erosion with increasing chamber pressure (for 300 V discharge). These trends are observed not only in the Mo data presented above but in the Mo data of surface layer activation tests (Ref. 11). It is unclear from this test campaign whether the prediction of significantly higher (4 times) IFPC erosion at lower discharge currents (Ref. 11) would be realized on graphite, but sensitivities to magnetic field and to discharge voltage were shown to be significantly smaller for graphite than Mo data would suggest.

5.0 Conclusion

A series of short duration wear tests were undertaken with two HERMeS technology demonstration units, TDU-1 and TDU-3. Wear and performance trends were characterized as a function of discharge voltage, magnetic field strength, facility pressure, and, to some extent, TDU configuration. Each test was roughly 200 h in length.

The keeper electrode in TDU-3 exhibited unexpected erosion which was largely independent of discharge voltage. Higher magnetic field strength increased keeper erosion rates. However, the keeper in TDU-1 which was located slightly upstream of the location of that in TDU-3, did not erode and showed net deposition. This is consistent with the lack of keeper erosion seen in the 2016 1700 h wear testing of TDU-1 and suggests the TDU-1 configuration should be used going forward. Sensitivity of the TDU-1 configuration to magnetic field remains to be determined.

Weak dependencies on discharge voltage and magnetic field were noted for inner front pole cover erosion. However a strong dependence on facility pressure was measured. With one outlying set of data which shows several trends inconsistent with physical explanation, higher facility pressure was shown to significantly decrease IFPC erosion. Comparison of Mo and graphite regression rates on the inner front pole covers suggests that the eroding ions are impacting with very high angles of incidence. However, the erosion profiles themselves suggest the ions are impacting at near-normal angles of incidence. It is likely that the uncertainties in the regression rate data are sufficient to accommodate extrapolation of the ratios of rates to regions of near-normal incidence and regions of larger angles of incidence which would coincide with the data.

Other components exhibited wear consistent with expectations. No erosion or cracking of the BN channel was seen. The TDU-3 outer front pole cover exhibited erosion rates near the detection threshold of the measurement, but higher than that observed in the TDU-1 wear testing. Deposition on the anode spalled during venting of VF-5 after about 500 h of operation. This spalling was not observed on TDU-1 operation in either VF-5 or VF-6 operation.

References

1. National Aeronautics and Space Administration Transition Authorization Act of 2017.
2. NASA Advisory Council Human Exploration and Operations Committee Meeting, https://www.nasa.gov/sites/default/files/atoms/files/nac_heoc_march_2017_public_agenda_revb.pdf, March 28-29, 2017, NASA Headquarters, Washington, DC.
3. Gerstenmaier, Bill, "Progress in Defining the Deep Space Gateway and Transport Plan," https://www.nasa.gov/sites/default/files/atoms/files/nss_chart_v23.pdf, NASA Advisory Council Human Exploration and Operations Committee Meeting, March 28-29, 2017, NASA Headquarters, Washington, DC.
4. Herman, D. A., et al., "Overview of the Development and Mission Application of the Advanced Electric Propulsion System (AEPS)," 35th International Electric Propulsion Conference, IEPC-Paper 2017-384, October 2017.
5. Hofer, R. R., et al., "Development Risks and Design of the 12.5 kW HERMeS Hall Thruster for the Solar Electric Propulsion Technology Demonstration Mission," 62nd JANNAF Propulsion Meeting, June 2015.
6. Kamhawi, H., et al., "Performance and Stability Characterization Tests of NASA's 12.5-kW Hall Effect Rocket with Magnetic Shielding Thruster," Proceedings of the 52nd Joint Propulsion Conference, AIAA Paper 2016-4826, July 2016.
7. Shastry, R., Huang, W., and Kamhawi, H., "Near-Surface Plasma Characterization of the 12.5 kW NASA TDU-1 Hall Thruster," 51st AIAA/ASME/SAE/ASEE Joint Propulsion Conference and Exhibit, July 27-29, 2015, Orlando, FL. AIAA-2015-3919.
8. Williams, G. J., and Kamhawi, H., "Optical Characterization of Component Wear and Near-Field Plasma of the HERMeS Thruster," Proceedings of the 51st Joint Propulsion Conference, AIAA Paper 2015-5025, July 2015.
9. Williams, G. J., et al., "Wear Testing of the HERMeS Thruster," Proceedings of the 52nd Joint Propulsion Conference, AIAA Paper 2016-5025, July 2016.
10. Mikellides, I. G., Ortega, A. L., and Jorns, B., "Assessment of Pole Erosion in a Magnetically Shielded Hall Thruster," 50th AIAA/ASME/SAE/ASEE Joint Propulsion Conference and Exhibit, July 28-30, 2014, Cleveland, OH. AIAA-2014-3879.
11. Polk, J., et al., "Inner Front Pole Erosion in the 12.5 kW HERMeS Hall Thruster Over a Range of Operating Conditions," 35th International Electric Propulsion Conference, IEPC-Paper 2017-409, October 2017.
12. Goebel, D., Jorns, B., Hofer, R., Mikellides, I., and Katz, I., "Pole-piece Interactions with the Plasma in a Magnetically Shielded Hall Thruster," 50th AIAA/ASME/SAE/ASEE Joint Propulsion Conference and Exhibit, Cleveland, OH, July 28-30, 2014. AIAA-2014-3899.
13. Chaplin, V., et al., "Laser Induced Fluorescence Measurements of the Acceleration Zone in the 12.5 kW HERMeS Hall Thruster," 35th International Electric Propulsion Conference, IEPC-Paper 2017-229, October 2017.
14. Gilland, J. H., Williams, G. J., Burt, J. M., and Yim, J., "Carbon Back-Sputter Modeling for Hall Thruster Testing," Proceedings of the 52nd Joint Propulsion Conference, AIAA Paper 2016-4941, July 2016.
15. Jorns, B. A., et al., "Mechanisms for Pole Piece Erosion in a 6-kW Magnetically-Shielded Hall Thruster," Proceedings of the 52nd Joint Propulsion Conference, AIAA Paper 2016-4839, July 2016.

16. Kamhawi, H., et al., "Performance and Stability Characterization of the HERMeS Thruster with M26 Boron Nitride Discharge Channel," 35th International Electric Propulsion Conference, IEPC-Paper 2017-392, October 2017.
17. Goebel, D., Jameson, K., and Hofer, R., "Hall Thruster Cathode Flow Impact on Coupling Voltage and Cathode Life," *Journal of Propulsion and Power*, Vol. 28, 2012, pp. 355-363.
18. Peterson, P. Y., et al., "NASA Glenn Research Center Vacuum Facility 6 Reconfiguration for HERMeS and AEPS Programs," 35th International Electric Propulsion Conference, IEPC-Paper 2017-028, October 2017.
19. Peterson, P. Y., et al., "NASA HERMeS Hall Thruster Electrical Configuration Characterization," Proceedings of the 52nd Joint Propulsion Conference, AIAA Paper 2016-5027, July, 2016
20. Soulas, G. C., "The Impact of Back-Sputtered Carbon on the Accelerator Grid Wear Rates of the NEXT and NSTAR Ion Thrusters," 33rd International Electric Propulsion Conference, IEPC-2013-157, October 2013.
21. Yim, John, "A Survey of Xenon Ion Sputter Yield Data and Fits Relevant to Electric Propulsion Spacecraft Integration," 35th International Electric Propulsion Conference, IEPC-Paper 2017-060, October 2017.
22. Oyarzabal, E., "Molybdenum and Carbon atom and carbon cluster sputtering under low-energy noble gas plasma," Ph.D. Dissertation, Engineering Physics, University of California, San Diego, 2008.